Computers and Concrete, Vol. 8, No. 5 (2011) 541-561
DOI: http://dx.doi.org/10.12989/cac.2011.8.5.541

Modelling seismically repaired and retrofitted reinforced concrete shear walls

W. Leonardo Cortés-Puentes and Dan Palermo*

Department of Civil Engineering, University of Ottawa, 161 Louis Pasteur, Ottawa, ON, Canada, K1N 6N5

(Received March 9, 2010, Revised August 17, 2010, Accepted September 8, 2010)

Abstract. The Finite Element Method (FEM) was employed to demonstrate that accurate simulations of seismically repaired and retrofitted reinforced concrete shear walls can be achieved provided a good analysis program with comprehensive models for material and structural behaviour is used. Furthermore, the analysis tool should have the capability to retain residual damage experienced by the original structure and carry it forward in the repaired and retrofitted structure. The focus herein is to provide quick, simple, but reliable modelling procedures for repair and retrofitting strategies such as concrete replacement, addition of diagonal reinforcing bars, bolting of external steel plates, and bonding of external steel plates and fibre reinforced polymer sheets, thus illustrating versatility in the modelling. Slender, squat, and slender-squat shear walls were investigated. The modelling utilized simple rectangular membrane elements for the concrete, truss bar elements for the steel and FRP retrofitting materials, and bond-link elements for the bonding interface between steel or FRP to concrete. The analyses satisfactorily simulated seismic behaviour, including lateral load capacity, displacement capacity, energy dissipation, hysteretic response, and failure mode.

Keywords: finite element modelling; reinforced concrete shear walls; seismic repair; seismic retrofitting; non-linear finite element analysis.

1. Introduction

Reinforced Concrete (RC) shear walls have been widely used in engineering practice as the main seismic force resisting system, while, at the same time, modern seismic design codes have evolved to include new requirements for the design and construction of shear walls, partly due to observed behaviour of structures in major earthquakes, and partly due to the understanding of the importance of ductility. This has resulted in explicit provisions to provide adequate ductility, and stringent reinforcement detailing requirements to prevent non-ductile modes of failure, while promoting flexural-related behaviour. The new detailing requirements can be readily incorporated in the design of new structures; however, this poses a significant challenge to the large inventory of existing structures designed and built according to earlier seismic codes. Therefore, reliable and cost-effective retrofitting techniques have emerged in an attempt to satisfy new design requirements for improved seismic performance. In addition, repair methodologies have also emerged as a means to restore damaged structures, which may have not been retrofitted before a seismic event. Research, particularly experimentally based, has been geared toward investigating and assessing diverse repair and retrofitting techniques. Lagging has been complementary analytical tools, which would provide

* Corresponding author, Assistant Professor, E-mail: Palermo@eng.uottawa.ca

an economical alternative to assess various repair and retrofitting schemes, allowing a systematic evaluation of different design parameters. Numerous procedures have been used to model strengthening of concrete structures prior to damage to varying degrees of success, such as Arduini *et al.* (1997) and Aprile *et al.* (2001) who modeled retrofitting of beams; and Li *et al.* (2005) who modelled retrofitting of shear walls, to name a few. Elnashai and Pinho (1998) performed non-linear analyses of retrofitted RC shear walls using the FEM; the walls were represented by cubic inelastic finite elements that were subdivided into fibres following the layered approach. Taghdi *et al.* (2000a) developed truss models for the analysis of retrofitted RC shear walls under monotonic loading based on the lower bound approach of the theory of plasticity. Limited research has been geared toward modelling of concrete structures after repair and retrofitting. Successful simulations require the capability to retain damage in the original structure and carry it forward in the repaired and retrofitted structure. Vecchio and Bucci (1999) introduced a FE simulation procedure for repairing/retrofitting concrete structures through engaging and disengaging elements in a structure, which models the sequence of construction and/or the implementation of the repair/retrofit scheme.

2. Research significance

Significant advancements in the FEM have provided capabilities to perform reliable analysis of repaired and retrofitted concrete structures. There is a need, however, to demonstrate how such procedures can be effectively used to provide quick, simple, yet reliable simulations of seismically repaired and retrofitted reinforced concrete structures. This paper presents nonlinear finite element analyses, and demonstrates the necessity of using a well-established numerical tool that utilizes comprehensive models for material and structural behaviour, and is capable of retaining damage experienced in a structure which must be carried forward to properly capture the behaviour after repair and retrofitting. The analyses include representative repair and retrofitting techniques for reinforced concrete shear walls including: replacement of concrete, addition of reinforcing bars, external bolting and bonding of steel plates, and external bonding of FRP sheets. Satisfactory results are obtained, while maintaining simplicity in the finite element model. Furthermore, guidance is provided for more detailed analyses to capture subtleties in behaviour.

3. Finite element modelling

3.1 Conceptual model

For this study, analyses were performed using VecTor2, a two-dimensional nonlinear finite element program applicable to membrane structures. This tool was chosen due to its capabilities to model the chronology of construction such as repair and retrofitting.

Program VecTor2 is based on the Modified Compression Field Theory (MCFT) and the Disturbed Stress Field Model (DSFM). The MCFT (Vecchio and Collins 1986) is a theory for predicting the load-deformation response of membrane elements subjected to shear and normal stresses. Cracked concrete is modelled as a solid continuum orthotropic material using a smeared rotating crack approach. The DSFM (Vecchio 2000b) represents an extension of the MCFT in several important aspects. Most importantly, the DSFM augments the compatibility relationships of the MCFT to

include crack shear-slip deformations. The strains due to these deformations are explicitly evaluated and separated from the strains of the concrete continuum due to stress. As such, the DSFM decouples the orientation of the principal stress field from that of the principal strain field. The DSFM was used for the analyses presented in this paper. A description of the constitutive models and finite elements available in VecTor2 that were used herein follows. Additional details can be found elsewhere (Wong and Vecchio 2002).

3.2 Smeared reinforced concrete

Concrete elements with smeared reinforcement were modelled with plane stress rectangles, a four-node element with eight degrees of freedom; two degrees of freedom at each node. The rectangle has constant thickness and its edges are parallel to the x and y axes. Constant strain triangular elements are also available and are generally used in regions where geometric constraints dictate.

The constitutive relationships for concrete are based on nonlinear empirical relations between stress and strain that describe the primary response as well as secondary effects of concrete behaviour. The program default constitutive models for concrete were used, except for the pre-peak and post-peak compression response of concrete; and the hysteretic response of concrete. The pre- and post-peak compression response was based on recommendations by Palermo and Vecchio (2007) and a parametric study conducted by Cortés-Puentes (2009), which included three common compression models: Popovics (Popovics 1973) normal strength (NSC), Popovics (Collins and Porasz 1989) high strength (HSC), and Smith-Young (Smith and Young 1955); and two post-peak models: base curve and modified Park-Kent model (Park, Priestly and Gill 1982). The base curve option uses the full stress-strain response of the chosen pre-peak model. In general, Popovics NSC model provided satisfactory results for normal strength concrete (strength less than 45 MPa), while Popovics HSC was the most suitable for high strength concrete (strength exceeding 45 MPa). The latter better predicts the stiffer pre-peak response and sudden strength decay in the post-peak region of high strength concrete. However, the studies also showed that the Smith-Young model is generally better at capturing the gradual softening response that is exhibited in the post-peak range of lower concrete strengths, and the post-peak modified Park-Kent model provides improved results for shear walls with confined boundary elements, which experience an increase in compressive strength due to the confining reinforcement. Therefore, based on the two studies, Popovics NSC was used for the shear walls with concrete strength not exceeding 45 MPa, while Popovics HSC was used for walls with concrete strength exceeding 45 MPa. The only exceptions were Walls B11/B11R and W11/W11RP. Wall B11/B11R contained confined boundary elements and the post-peak modified Park-Kent model provided the most accurate results. For Wall W11/W11RP, with a concrete compressive strength of 29 MPa, the Smith-Young model was able to more accurately simulate the gradual softening in the post-peak response.

Cortés-Puentes (2009) also conducted a parametric study of two concrete hysteretic models: the nonlinear default model and the nonlinear with cyclic decay model (Palermo and Vecchio 2003). The latter is an improvement relative to the default model; it accounts for stiffness and strength degradation of the reloading branches, considers partial unloading/reloading, and provides an improved estimate of the plastic offset. The study demonstrated marginal differences between the two models for flexural dominant walls; however, the Palermo and Vecchio model provides improved results for walls controlled by shear deformations. Thus, the Palermo and Vecchio model was selected for the hysteretic response of concrete.

The default models were selected to account for secondary effects. Compression softening, which accounts for the reduction in compressive strength and stiffness due to coexisting transverse tensile straining was modelled with Vecchio's 1992-A model (Vecchio and Collins 1993). Tension stiffening was modelled by the modified Bentz model (Vecchio 2000b), which determines the tensile stresses that exist in concrete between cracks due to the bond action between the reinforcement and the concrete. The post-cracking tensile stresses present in plain concrete, known as tension softening, was modelled with a linear descending response after cracking (Vecchio 2000b). The lateral expansion of concrete caused by internal micro cracking, which increases as the compressive stresses increase, was modelled with a variable Poisson's ratio based on the work of Kupfer (Kupfer *et al*. 1969). The concrete confined strength enhancement was captured with the Kupfer/Richart model. The Kupfer *et al*. (1969) formulation, which models the strength enhancement in a bi-axial compression state, was extended to include the strength enhancement effect noted in spiral columns by Richart *et al*. (1928), resulting in a model for the strength enhancement in a tri-axial compression state (Vecchio 1992). The cracking strength of concrete which can differ from the concrete tensile strength due to co-existing transverse compressive stresses was considered with the Mohr-Coulomb stress criterion. Consideration was also given to the width of cracks, which can cause a reduction in the compressive strength when crack widths exceed a specified limit; a limit of 20% of the aggregate size was used (Vecchio 2000a). The crack shear-slip deformations, which represent the main compatibility feature of the DSFM was evaluated with the Vecchio-Lai model (Vecchio and Lai 2004).

3.3 Discrete reinforcement

Two-node truss bars with uniform cross-sectional area were used to model internal and external reinforcement where the reinforcement was not modelled as smeared. The truss bar element has four degrees of freedom; displacement in x and y directions at each node, and can assume any orientation in the x, y coordinate system. Three materials were assigned depending on the type of reinforcement: ductile steel reinforcement; externally bonded FRP reinforcement; or tension only reinforcement. Ductile steel reinforcement was used for internal steel reinforcement modelled discretely and for external steel plates that were bonded or bolted as part of the retrofitting process. The externally bonded FRP was used to model horizontal FRP sheets. The tension only reinforcement was implemented to simulate the behaviour of vertical FRP strips. The stress-strain response of the FRP is similar to the tension only reinforcement model; however, modifications permit local crack stresses to be more accurately calculated.

The Seckin Model (Seckin 1981, Vecchio 1999) was selected to capture the hysteretic response of the reinforcement. The model includes a linear elastic region followed by a yield plateau and strain hardening. The unloading and reloading response includes the Bauschinger effect. Dowel action of the reinforcement, which arises from crack slip occurring transversely to the axes of the reinforcement, was considered using the Tassios crack slip model (Vintzelou and Tassios 1987, He and Kwuan 2001). Buckling of internal reinforcement was not considered in order to reduce the number of elements and to maintain simplicity in the finite element models. This requires modelling the reinforcement as discrete truss bars and employing bond-link elements between the truss bar elements and the concrete elements in Program VecTor2. Even though buckling of the internal reinforcement has been observed in some tests (Taghdi *et al.* 2000b), the perfectly bonded reinforcement assumption provided satisfactory results, while reducing the required number of

elements and maintaining simplicity of the finite element model. Similar conclusions were noted by Palermo and Vecchio (2007). However, it has been noted that some of the analysis results could be improved with the inclusion of bar buckling including the predicted failure mode.

3.4 Bonding interface

To simulate the effect of bond between external reinforcement and concrete, a two node non-dimensional link element was used. The link element connects the concrete element to the truss bar, which represents the external bonded element. The link element contains two orthogonal springs to connect the nodes of the truss bar and concrete element located at the same coordinate; this allows for transferring of shear and normal stresses to the reinforcement. The bond-link behaviour of the externally bonded steel and FRP was modelled with a linear elastic ascending response, followed by a linear post-peak descending branch based on the fracture energy method (Sato and Vecchio 2003). In addition, the Eligehausen model (Eligehausen *et al*. 1983) was used to capture the hysteretic response of the element.

3.5 Modelling and analysis of the repair/retrofitting construction process

Simulation of a repaired and retrofitted concrete structure requires the capability to model the chronology of the repair and retrofitting process and ensuring that any residual damage prior to repair/retrofitting is carried forward. Program VecTor2 has such capabilities through the process of engaging and disengaging elements (Vecchio and Bucci 1999), while retaining residual strains. Engaged elements represent portions of the structure that are currently present and contribute to the strength and stiffness. Conversely, disengaged elements represent portions of the structure that are currently absent and do not contribute to the strength and stiffness. Fig. 1 is a schematic representing the modelling process, where a shear wall is tested and then repaired by replacing damaged concrete in the lower half of the wall, followed by retrofitting through wrapping a horizontal sheet of FRP around the wall. Note that the concrete is represented by rectangular

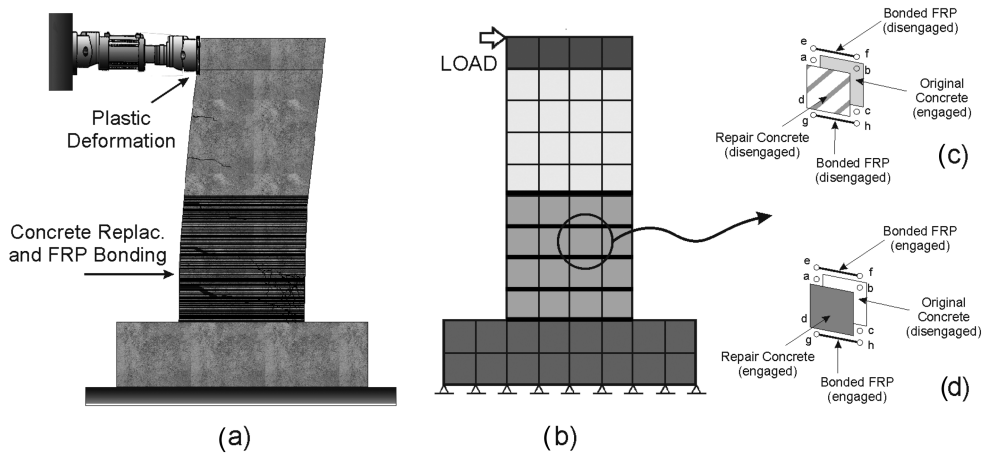

Fig. 1 Modelling of repaired/retrofitted shear wall: (a) specimen, (b) FE Model, (c) detail of original wall and (d) detail of repaired/retrofitted wall

elements, while truss bar elements are used to simulate the FRP. The original structure is analyzed by engaging elements representing the original material, while elements representing repair and retrofitting materials are initially disengaged. The disengaged elements are superimposed over the engaged elements that they replace during repair and retrofitting, thus they share the same coordinates. During simulation of the repair/retrofitting, the elements of the original structure that are damaged and removed during repair and retrofitting are disengaged, while the elements representing the repair and retrofit are engaged. This process ensures that the total strain in both the engaged and disengaged elements sharing the same position is identical. After analysis of the original structure, the total strain of the disengaged repair/retrofit element is retained as a plastic offset strain and is carried forward in the analysis of the repaired/retrofitted structure. The net strain, however, of the element representing the repair/retrofit material is zero when it becomes engaged, reflecting the actual repair/retrofitting condition of placing a new material with no stress. Subsequently, in the analysis of the repaired structural model, the newly engaged elements contribute to the strength and stiffness. Elements from the original structure which remain engaged carried forward any residual damage.

3.6 Finite element mesh

The finite element mesh of the shear walls consisted of a minimum of 13 rectangular plane stress elements in the short direction including the boundary elements, while maintaining an aspect ratio of 3 to 2, unless geometric constrains dictated otherwise, following the suggestions of (Palermo and Vecchio 2007). Meshing of the foundation and top beams of the shear walls conformed to the mesh of the walls. Nodes at the bottom of the foundation mesh were restrained in the x and y directions to simulate the fixed support condition of the shear wall. Sufficiently fine meshes were used in the models to ensure accurate simulation of the strain and stress gradients across the length of the walls. Note that the concrete elements are based on a linear displacement field (constant strain elements). The lateral loading and axial loading, if present, employed in the analyses were consistent with that imposed during testing of the shear walls, and were applied along the top loading beams.

4. Fem analysis case studies

Walls repaired and retrofitted with different techniques were simulated including replacement of concrete, addition of diagonal steel reinforcing bars, external bolting of steel plates, and external bonding of steel plates and FRP sheets. provides details of the material properties of the shear walls discussed in the following sections.

4.1 Concrete replacement

Walls B11/B11R (Fiorato *et al.* 1983) represented slender walls with barbell sections and dimensions of 4570 mm in height, 1910 mm in length, and 102 mm in thickness (Fig. 2). The boundary columns were 305 mm × 305 mm. In addition, the walls were built with stiff top and foundation beams. Wall B11 was repaired (Wall B11R) by removing concrete in the web from the foundation beam up to a height of 2600 mm and replacing it with high strength concrete. In the boundary elements, where spalling of concrete was observed, roughening, removing of loose particles, and subsequent hand-

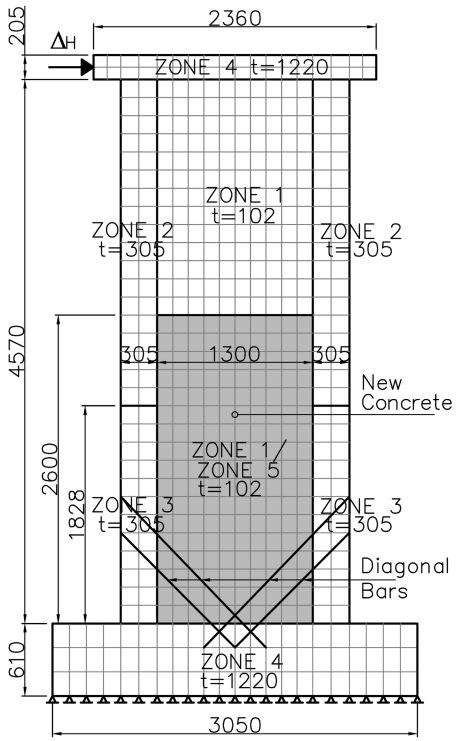

Fig. 2 Finite element mesh of Walls B11/B11R. All dimensions in mm

packing of a sand-cement mortar was applied. The wall was further retrofitted by placing four diagonal reinforcing bars (two in each direction) near the base of the wall as shown in Fig. 2. The original reinforcement in Wall B11 remained intact.

The FE model for Walls B11/B11R consisted of five concrete zones, as illustrated in Fig. 2 : the web wall (zone 1); upper (zone 2) and lower (zone 3) portion of the boundary elements (the latter with more transverse and confinement reinforcement); the foundation and top beams (zone 4); and the repair concrete in the lower portion of the web wall (zone 5). All the vertical, horizontal and confinement reinforcement was smeared in the concrete. The model contained 692 rectangular concrete elements. The four diagonal bars included in the retrofitting were modelled as ductile truss bars, and were assumed perfectly bonded to the foundation and boundary elements only. The repair and retrofitting was simulated by engaging the repair concrete (zone five) and diagonal truss bars, and disengaging the elements representing the removed concrete (zone one). The repair simulation did not include the concrete hand-packing of the boundary elements.

The observed hysteretic response of the original wall, B11, is illustrated in Fig. 3. The wall first yielded at 25 mm of displacement which occurred during an initial long loading cycle to 95 mm of displacement. While loading to the third repetition to 126 mm, prior to failure, the wall attained maximum lateral strength capacity of 726 kN. Failure was characterized by significant crushing of concrete in the web wall. Substantial shear distortion was also observed near the base of the wall at the end of testing. The wide hysteretic cycles indicate that the wall dissipated significant energy, while the displacement ductility of approximately 5.0 indicates ductile behaviour. By replacing the damaged concrete and adding diagonal reinforcing bars in Wall B11R, the peak strength and

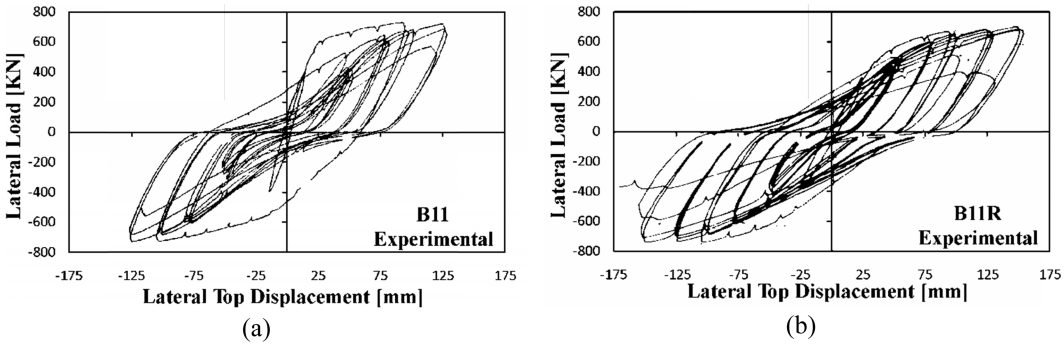

Fig. 3 Experimental load-deformation responses: (a) Wall B11 and (b) Wall B11R (Modified from Fiorato *et al.* 1983)

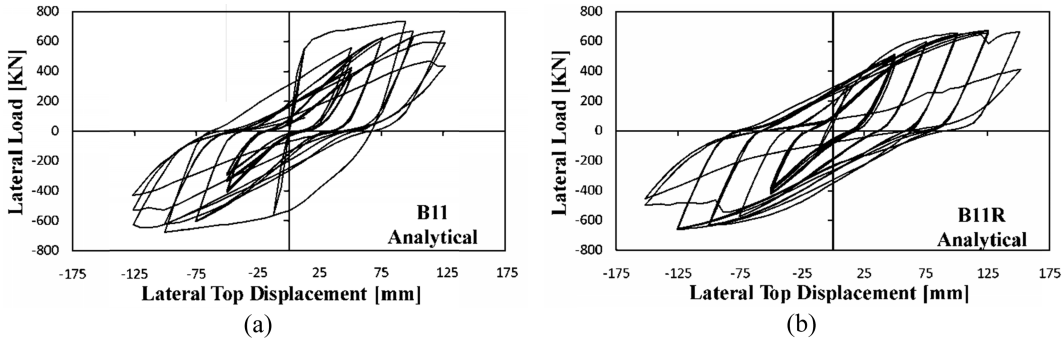

Fig. 4 Numerical load-deformation responses: (a) Wall B11 and (b) Wall B11R

displacement capacity were increased as shown in Fig. 3. The improvements in strength and ductility were mainly due to the bi-diagonal bars, which increased the shear capacity of the section, thus delaying failure.

The predicted response of the original wall, B11, (Fig. 4) was in good agreement with the observed response. Behavioural aspects such as lateral strength, ductility, and energy dissipation were accurately captured. Maximum strength capacity of 735 kN was predicted during the initial long loading cycle to 95 mm of displacement. Subsequent cycles captured the stiffness degradation, unloading and reloading branches, and the pinching effect. The analysis correctly simulated failure in form of crushing of concrete in the web wall during the third repetition to 126 mm of displacement. The analysis satisfactorily simulated the response of the repaired wall, B11R, (Fig. 4). This was a result of properly simulating damage in the original wall, which was carried forward in the analysis of the repaired wall. The maximum strength of 672 kN slightly underestimated the recorded strength. This discrepancy is most probably due to the strain hardening modulus used in the analysis. Failure was predicted during the first excursion to 152 mm, whereas failure was reported at the same displacement but after multiple repetitions. The predicted unloading, reloading, and pinching effect compared well. The failure mode was well simulated; concrete crushing in web near the interface with the boundary elements, along with significant shear distortion.

Walls LSW3/RLSW3 (Salonikios *et al.* 1999, Antoniades *et al.* 2003) were squat reinforced concrete walls 1200 mm high, 1200 mm long, and 100 mm thick as illustrated in Fig. 5. The original wall, LSW3,

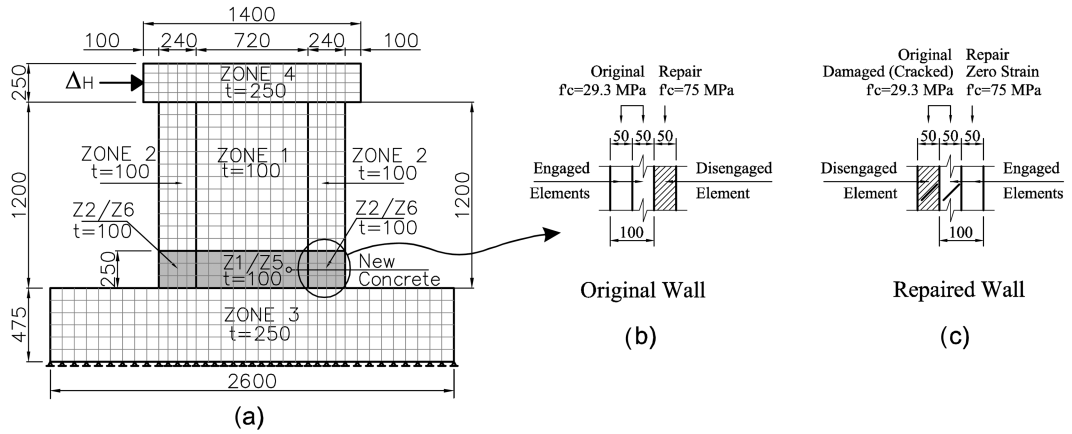

Fig. 5 Finite element mesh of Walls LSW3/RLSW3: (a) meshing, (b) detail of partial replacement for original wall and (c) detail of partial replacement for repaired wall. All dimensions in mm

was cyclically loaded to failure and then repaired (RLSW3) by removing heavily damaged concrete within the lower 250 mm of the wall, including the boundary elements; replacing damaged vertical reinforcement and hoops; and casting of new high strength nonshrink mortar with compressive strength of 75 MPa and modulus of elasticity of 25000 MPa. Damaged vertical reinforcement was replaced with new reinforcing bar segments and lap welded to the remaining reinforcement.

Walls LSW3/RLSW3 were modelled with 626 concrete elements with smeared reinforcement, including 68 elements to simulate the repair mortar at the base of the wall. The finite element model, depicted in Fig. 5, was divided into six concrete zones corresponding to the web (zone 1), boundary elements (zone 2), foundation beam (zone 3), top beam (zone 4), and repair mortar in the lower 250 mm of the web and boundary elements (zone 5 and 6, respectively). At the end of the analysis of the original wall, the concrete removed in the lower 250 mm of the web and boundary elements was simulated by disengaging the damaged elements present in the repair zone (zone 1). Casting of the new high strength repair mortar was simulated by engaging the elements of zone 5 and 6. This modelling sequence assumed full through-thickness replacement of the damaged concrete. Disengaging the smeared concrete in zone 1 implicitly removed the reinforcement in this zone, while engaging the new smeared mortar elements in zone 5 and 6 provided new reinforcement.

Fig. 6 illustrates the rounded response of the original wall, LSW3, where the wall sustained stiffness and strength degradation until failure. Peak strength of 268 kN was reported at a lateral displacement of 4 mm (Salonikios *et al.* 1999). Thereafter, the wall experienced a gradual reduction in strength capacity until failure. Failure, in the form of shear sliding (horizontal sliding) at the base of the wall, was reported at 15 mm of displacement. Prior to shear sliding, crushing of concrete, specifically in the boundary elements was visible. The original wall responded with sufficient energy dissipation, although the hysteretic response indicated some degree of pinching, which reflected the horizontal sliding along the base. The response of the repaired wall, RLSW3, (Fig. 6) displayed smaller initial stiffness, strength capacity, and ductility compared to the original wall. The energy dissipation was not recovered, and the hysteretic loops were more pinched. The wall attained peak strength of 179 kN at a displacement of 6 mm, beyond which the wall responded with significant strength degradation. The test was terminated at 14 mm of displacement. Antoniades *et al.* (2003) did not explicitly report the failure mode of Wall RLSW3, but the post-peak response in

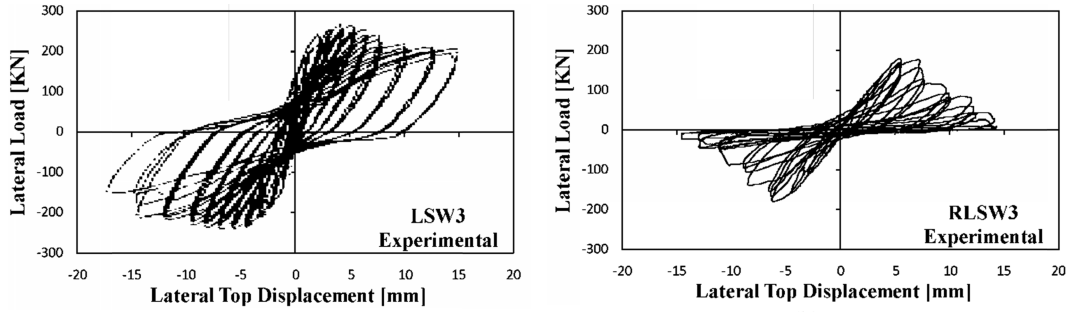

Fig. 6 Experimental load-deformation responses: (a) Wall LSW3 and (b) Wall LSW3R (Modified from Salonikios *et al.* 1999 and Antoniades *et al.* 2003)

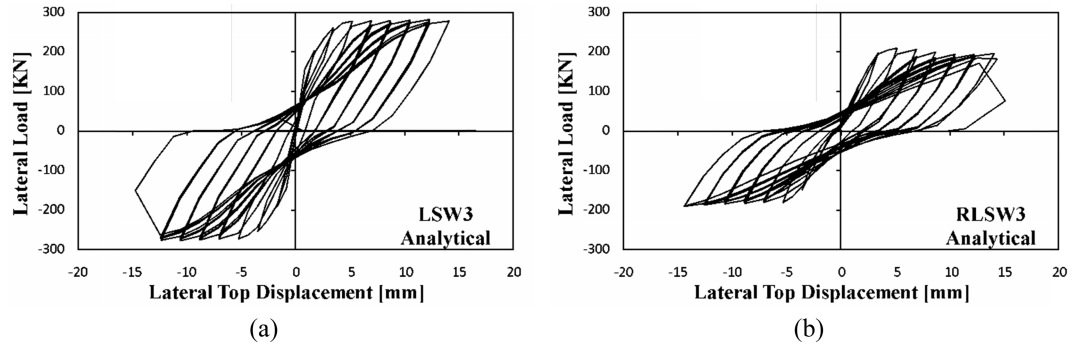

Fig. 7 Numerical load-deformation responses: (a) Wall LSW3 and (b) Wall LSW3R

Fig. 6 indicates concrete degradation (crushing) along with shear sliding.

The predicted response of Wall LSW3 (Fig. 7) accurately captured the pre-peak response; however, the analysis underestimated the stiffness and strength degradation in the post-peak range. The initial stiffness and yielding at 4 mm closely matched that reported. The predicted peak strength of 282 kN was in good agreement, although the corresponding lateral displacement of 14 mm was overestimated. The analysis did not capture the concrete softening in the post-peak range, which resulted from loss of cross section associated with probable buckling of the vertical reinforcement. This discrepancy, however, did not affect the satisfactory prediction of pinching. Shear sliding failure at the base of the wall was predicted at 14 mm, and correlated to that observed during testing. The post-peak response could be improved by employing a more detailed model with truss bars elements for the internal reinforcement and connected to the concrete elements with bond-link elements to capture buckling.

The analytical response of Wall RLSW3 (Fig. 7) overestimated the strength capacity and the ductility. Furthermore, the analysis overestimated the initial stiffness and did not capture the significant stiffness and strength degradation in the post-peak range. Failure was initiated by crushing of concrete, leading to shear sliding at the base of the wall, which was similar to that observed. Underestimation of the stiffness degradation resulted in less pinching. Discrepancies in the predictions, particularly in terms of initial stiffness and stiffness degradation, suggest partial replacement rather than complete replacement of the damaged concrete. Note that Antoniades *et al.* (2003) did not

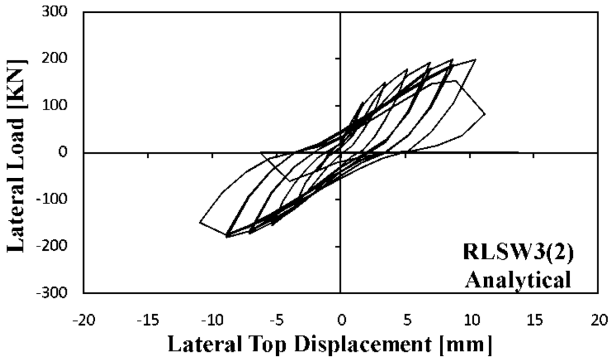

Fig. 8 Modified numerical load-deformation response for Wall RLSW3

provide a complete description of the repair construction process. A second analysis, named RLSW3(2), was performed with a triple mesh in the repair zone to simulate partial concrete replacement, as shown in Fig. 5. It was assumed that 50% of previously damaged concrete was removed and replaced by new high strength mortar. The procedure involved engaging the original concrete elements for the analysis of Wall LSW3. During repair, 50 mm of the original concrete was removed (disengaged), while a new 50 mm thick high strength mortar was added (engaged). Generally, the proposed modelling strategy for partial replacement of concrete provided better response of Wall RLSW3, as shown in Fig. 8. The initial stiffness, peak strength of 188 kN, and peak displacement of 9 mm were in better agreement; however, the stiffness and strength degradation in the post-peak range were underestimated.

4.2 External bonding of steel plates

Walls SW24/SWR24 were tested to investigate a shear-strength technique to improve ductility of a shear wall governed by shear-related mechanisms (Elnashai and Salama 1992, Elnashai and Pinho

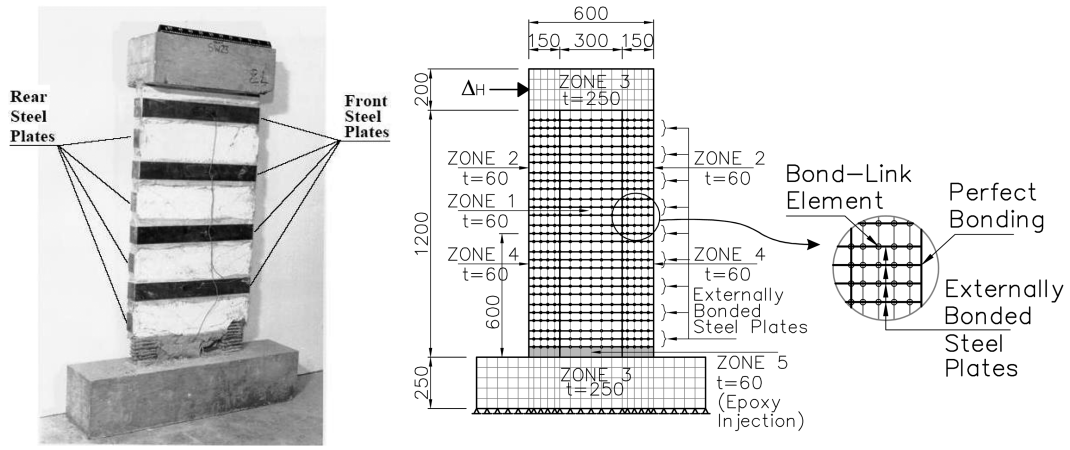

Fig. 9 Walls SW24/SWR24: (a) test specimen (Elnashai and Pinho 1998), (b) finite element mesh and (c) detail of bonded steel plates. All dimensions in mm

1998). Fig. 9 depicts the geometry of the walls, which were 1200 mm high, 600 mm long, and 60 mm thick. The walls included asymmetrical vertical reinforcement in each boundary element; larger bars were concentrated at the edges of the walls. Repair of the damaged wall (SWR24) involved injection of the cracks with a high strength epoxy. Retrofitting consisted of bonding full length horizontal steel plates (78 mm wide and 3.6 mm thick) with epoxy resin on both sides of the wall in a staggered pattern. The plates were bent at the extremities and bonded to the edge of the wall.

The finite element model illustrated in Fig. 9 was constructed with 658 smeared concrete elements defining five concrete zones: the web (zone 1), the upper half of the boundary elements (zone 2), the foundation and top beams (zone 3), the lower half of the boundary elements (zone 4), and the bottom row of concrete elements in the wall to simulate the epoxy injection of cracks near the foundation beam (zone 5). Internal vertical reinforcement of the boundary elements was modelled with perfectly bonded truss bars to better represent the asymmetrical layout of the reinforcement. Each externally bonded steel plate was modelled with three horizontal rows of ductile truss bars connected to the concrete with bond-link elements to simulate the effect of slip. An exception was at the ends of the wall, where the steel plates were bent. At this location, the truss bars where modelled as perfectly bonded to the concrete elements. Fig. 9 provides a detail of the simulation of the externally bonded steel plates with bond-link elements. After the initial analysis of the virgin wall, the truss bars with bond-link elements representing the externally bonded steel plates, and concrete elements to simulate the crack injection were engaged, while the original concrete elements near the foundation beam were disengaged. Note that epoxy injection was simulated with complete replacement of the damaged elements, thus assuming perfect sealing of the cracks. The remainder of elements defining the web, boundary elements, and foundation and top beams remained engaged.

The non-ductile behaviour of the original wall, SW24, is evident in Fig. 10. The recorded response was asymmetrical and displayed stiffer hysteretic loops in the negative direction. Existing damage prior testing, due to transportation problems, resulted in a softening of the response in the positive direction. The wall sustained a maximum strength of 110 kN at 18 mm of displacement in the positive direction, and 125 kN at 12 mm of displacement in the negative direction. The response displayed significant pinching and low energy dissipation capacity. Failure was observed during the first repetition of loading to 21 mm of displacement and involved crushing of concrete in the web.

The repaired wall, SWR24, experienced improved ductility and energy dissipation capacity. The rounded response displayed signs of shear-related mechanisms governing the behaviour. Peak

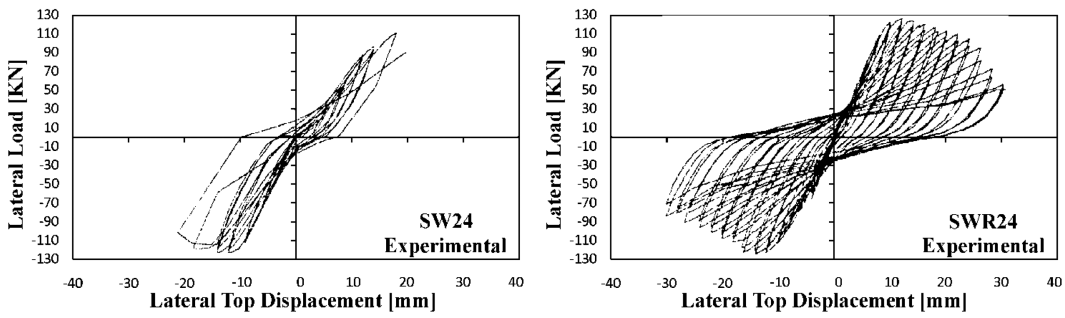

Fig. 10 Experimental load-deformation responses: (a) Wall SW24 and (b) Wall SWR24 (Modified from Elnashai and Salama 1992)

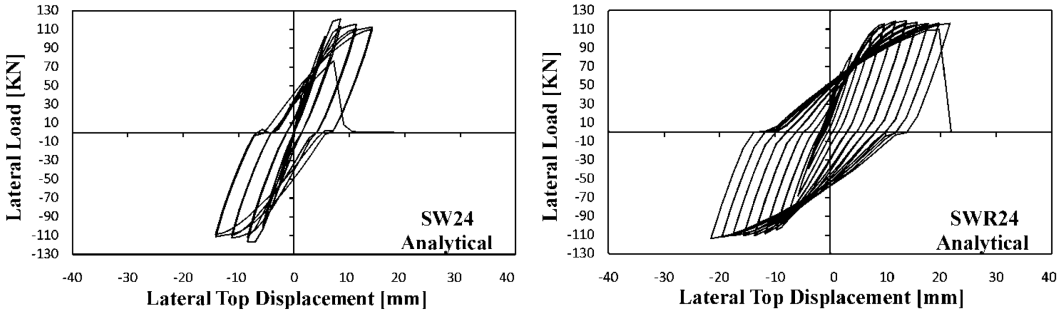

Fig. 11 Numerical load-deformation responses: (a) Wall SW24 and (b) Wall SWR24

strength of 125 kN was recorded at 10 mm of displacement. During the post-peak range, the wall sustained gradual stiffness and strength degradation, leading to crushing of concrete with high shear distortion, specifically in the boundary elements. The first steel plate, near the foundation beam, debonded at 20 mm of displacement.

The predicted response of the original wall, SW24, (Fig. 11) was in good agreement with the observed response, specifically in terms of strength and ductility. However, the analysis predicted higher initial stiffness. This discrepancy is due to the damage in the wall prior to testing, which was not considered in the analysis. Peak strength of 121 kN was predicted at 9 mm. The slightly wider hysteretic loops resulted in more energy dissipation compared to the observed response. Furthermore, the analysis predicted less pinching, which was associated with less damage due to shear stiffness degradation. Failure in the form of shear sliding was simulated during the first repetition to 16 mm of displacement. Note that shear sliding was preceded by crushing of the concrete at the bottom of the wall, which corresponded to the actual failure.

Fig. 11 shows the predicted response of the repaired and retrofitted wall, SWR24. The simulation predicted a recovery of the stiffness and lateral strength. The peak strength, 119 kN, was slightly underestimated, and the corresponding displacement of 19 mm was greater than the experimental response. The response flattened in the post-peak range and sustained the peak strength to failure. The analysis did not capture the stiffness and strength degradation in the post-peak range. However, unloading of the hysteretic loops was accurately captured. Failure to capture the stiffness degradation resulted in underestimation of pinching and overestimation of the total energy dissipation capacity. These discrepancies are probably due to the assumption of full replacement of concrete to simulate epoxy injection of cracks, which captured the recovery of the initial stiffness; however, it did not capture the shear stiffness degradation associated with re-opening of sealed cracks. Failure as a result of shear sliding was predicted at 22 mm of displacement, and was preceded by crushing of the concrete at the bottom of the wall.

4.3 External bolting of steel plates

Wall W11 reported by Taghdi *et al.* (2000b), a squat reinforced concrete shear wall 1800 mm in height, 1800 mm in length, and 100 mm in thickness, was tested and subsequently repaired (W11RP). Repair consisted of bolting two vertical steel plates (160 mm wide and 4.76 mm thick) near each end of the wall without treatment of the damaged concrete. Bolt spacing of 100 mm in

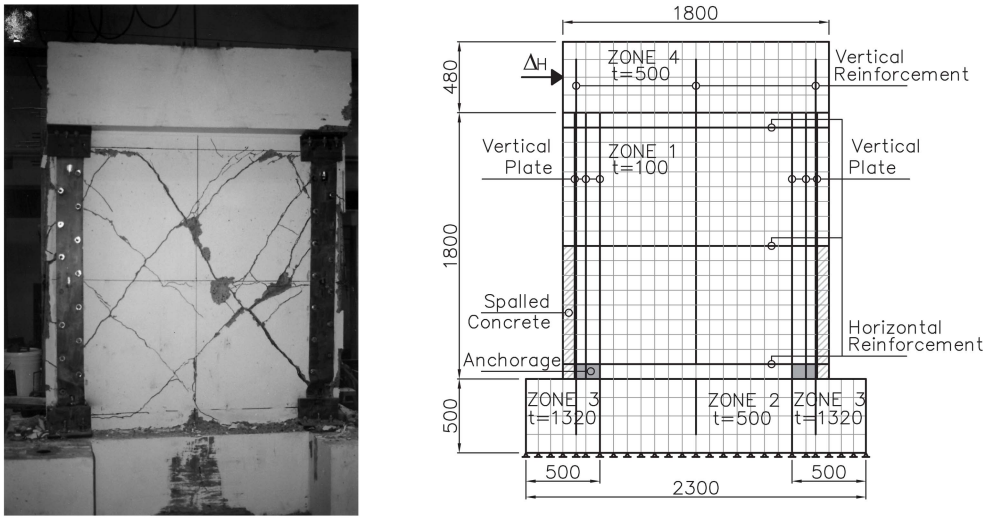

(a) (b)

Fig. 12 Walls W11/W11RP: (a) test specimen (Taghdi *et al.* 2000b) and (b) finite element mesh. All dimensions in mm

the vertical steel plates was chosen to prevent elastic buckling. The ends of the vertical steel plates were welded to 154 mm × 154 mm×x 15.9 mm steel angles, which were anchored to the foundation and top beam by means of 19 mm diameter anchor bolts. The repaired wall is shown in Fig. 12.

The FE model consisted of four concrete zones as depicted in Fig. 12: the plain concrete in the web (zone 1), which included truss bars to represent the internal vertical and horizontal reinforcement; the stiff I-shape foundation (zones 2 and 3); and the stiff top beam (zone 4). The internal reinforcement was discretely modelled to represent the actual location of the reinforcement. Note that smearing of this small area of reinforcement over wall surface would significantly underestimate the contribution of the reinforcement at its actual location. Each externally bolted steel plate was simulated with three vertical rows of 18 ductile truss bar elements perfectly bonded to the concrete near each end of the wall. A preliminary model with bond-link elements was investigated to capture buckling of the plates; however, this phenomenon was not well captured owing, in most part, to the bond-link properties not reflecting the bolting technique used to attach the steel plates to the concrete. The finite element mesh included 548 rectangular concrete elements. Furthermore, four stiff concrete elements were defined near the bottom corners of the wall to simulate anchorage of the steel plates to the foundation during the repair process. The repair and retrofit was simulated after the analysis of the original wall and included disengaging 18 concrete elements at the edges of the wall to simulate the observed spalling of concrete. Then, the truss bars defining the vertical steel plates, and the concrete elements defining the anchors to the foundation were engaged.

The original wall, W11, experienced yielding at approximately 0.2% lateral drift (Fig. 13). Thereafter, the wall sustained a clear yield plateau with marginal increase in strength capacity. The ultimate strength of 173 kN was recorded at 2.0% lateral drift. The wall behaviour was controlled by rocking at the base. This behaviour promoted crushing of concrete at the end of the walls and elastic buckling of the vertical reinforcing bars. This mechanism resulted in failure due to

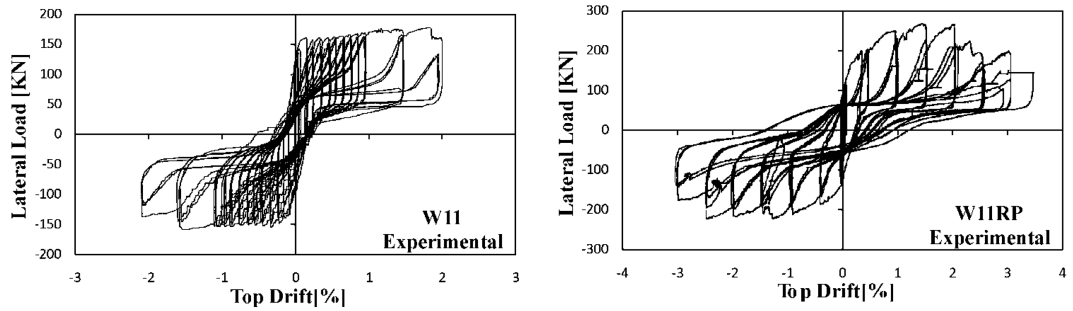

Fig. 13 Experimental load-deformation responses: (a) Wall W11 and (b) Wall W11RP (Modified from Taghdi *et al.* 2000b)

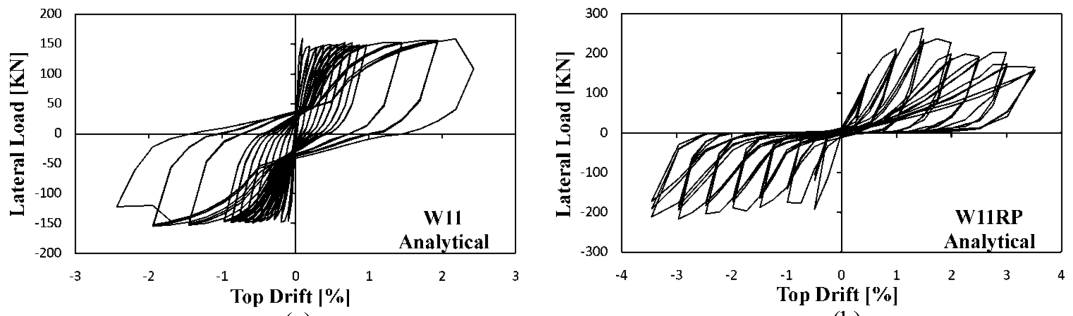

Fig. 14 Numerical load-deformation responses: (a) Wall W11 and (b) Wall W11RP

discontinuity of the construction joint between the web and foundation, and rupturing of the middle vertical reinforcing bars. The pinching of the hysteretic loops was associated with rocking. The repaired wall, W11RP, recovered the initial stiffness, and improved the strength capacity, ductility, and energy dissipation as shown in Fig. 13. The onset of plastic buckling of the steel plates was reported at 1.32% lateral drift, corresponding to a lateral strength of approximately 260 kN. The wall reached its peak strength of 269 kN at 1.5% lateral drift, and was sustained to 2.0% lateral drift. The wall sustained significant shear sliding at the base, which occurred simultaneously with slippage of the anchor bolts. Failure was reported during the first repetition to 2.5% lateral drift where the wall experienced a sudden drop in strength. The cracking pattern at the end of testing consisted of two wide diagonal cracks in each direction along with the existing horizontal cracks along the construction joint sustained by the original wall.

The analysis of the original wall, W11, accurately captured the initial stiffness as shown in Fig. 14. Yielding was predicted at 0.2% lateral drift. After yielding, the response flattened and gained marginal lateral strength, similar to that observed. The analysis predicted a maximum strength of 156 kN at 2.0% lateral drift, which slightly underestimated that recorded. Maximum displacement of 2.0% lateral drift, corresponding to a displacement ductility of approximately 10, was accurately predicted. During the first repetition to 2.5% lateral drift, the analysis predicted failure of the wall due to crushing of concrete at the ends of the wall coupled with high shear distortion. The analysis neither captured buckling nor rupturing of the vertical reinforcement. However, the analysis predicted crushing of the concrete elements surrounding the vertical reinforcement, which indicated

the buckling phenomenon. Cracking of the concrete elements surrounding the extreme vertical reinforcement corresponded to spalling of concrete observed during buckling. The predicted hysteretic loops differed somewhat to that reported. The unloading branch displayed gradual strength reduction, not observed, and the reloading branch predicted less stiffness degradation, specifically beyond 1.0% lateral drift. This discrepancy may be due to the analysis not accurately capturing the buckling of reinforcement and rocking behaviour along the construction joint. Note that the vertical reinforcement was assumed perfectly bonded to the concrete, thus the anchorage slip leading to the rocking motion was not modelled. Improvements could be achieved by using bond elements between the vertical internal reinforcement and the concrete elements.

Prior to the analysis of the repaired wall, W11RP, rupturing of the middle vertical reinforcing bars was simulated by disengaging the truss bar element representing this reinforcement near the foundation. The analytical response (Fig. 14) of the repaired wall was in good agreement with the recorded response in terms of strength capacity, and stiffness degradation. However, the analysis underestimated the initial stiffness and overestimated the pinching phenomenon. Peak lateral strength was accurately predicted in both directions; 264 kN at 1.5% lateral drift in the positive direction, and 217 kN at 3.0% lateral drift in the negative direction. The predicted failure mechanism consisted of concrete crushing with high shear distortion of the concrete elements representing the left anchorage plate, and shear sliding of the second row of concrete elements between 1.5% and 2.0% lateral drift. Beyond 2.0% lateral drift, the analysis predicted extensive damage in the concrete, and the strength capacity was limited to the contribution of the steel plates. Plastic buckling of the vertical steel plates was not captured, but the predicted shear distortion of the concrete elements crossing the truss elements defining the steel plates suggested this phenomenon.

4.4 External bonding of FRP sheets

Walls MSW1/FRPMSW1 (Antoniades *et al.* 2005) were squat-slender reinforced concrete walls

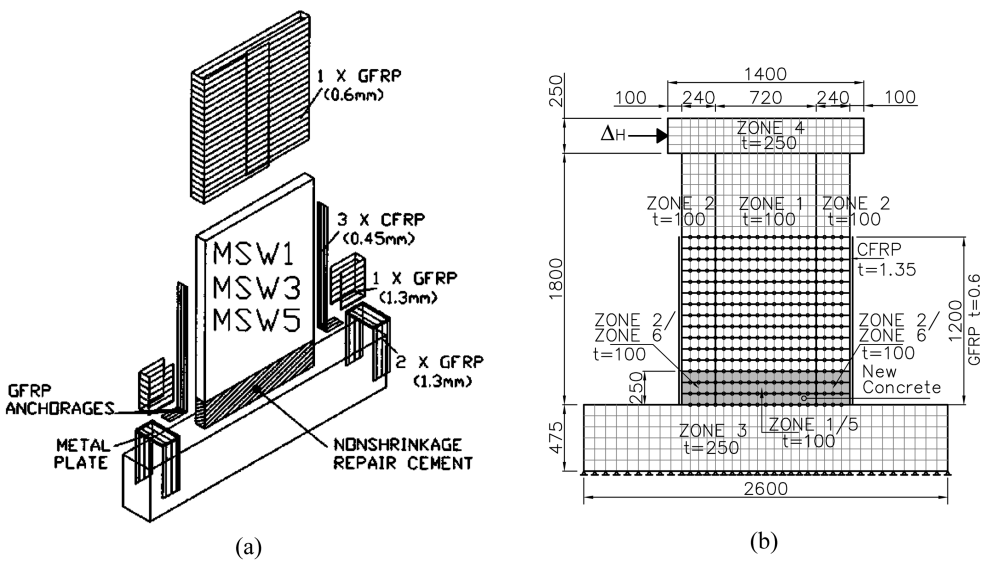

Fig. 15 Walls MSW1/FRPMSW1: (a) test specimen (Antoniades *et al.* 2005) and (b) finite element mesh. All dimensions in mm

with dimensions of 1800 mm in height, 1200 mm in length, and 100 mm in thickness as illustrated in Fig. 15. The original specimen, Wall MSW1, was cyclically loaded to failure, and subsequently repaired and retrofitted (FRPMSW1). Repair and retrofitting involved removing heavily damaged concrete within the lower 250 mm of the wall, including the boundary elements. In addition, damaged vertical reinforcement was cut and replaced with new reinforcing bar segments, and damaged hoops were also replaced. New nonshrink high strength mortar, similar to that used for Wall RLSW3, with compressive strength of 75 MPa and modulus of elasticity of 25000 MPa was then cast in the lower section of the wall. The retrofit involved application of three layers of 0.45 mm thick and 100 mm wide carbon fibre reinforced polymer (CFRP) strips at the edges of the wall with fibres oriented in the vertical direction. The strips were bent at the base of the wall and extended (development length) along the foundation for anchoring. GFRP C-shaped pieces of 1.3 mm thickness were placed over the strips at the lower part of the boundary column. This was followed by wrapping of the wall with 0.6 mm thick glass fibre reinforced polymer (GFRP) sheets over a height of 1200 mm. The development length of the edge FRP strips were anchored to the foundation with a combination of inverted U-shaped GFRP and a 20 mm thick steel plate glued with an epoxy resin.

The finite element model contained six concrete zones: web (zone 1), boundary elements (zone 2), foundation beam (zone 3), top loading beam (zone 4), and new repair mortar in the lower 250 mm of the web wall (zone 5) and boundary elements (zone 6). The total number of rectangular concrete elements used in the model was 728, in which 442 corresponded to the web and boundary elements and 51 for the simulation of the replacement of the concrete. Vertical CFRP strips were modelled with 30 perfectly bonded tension only truss bar elements (15 at each wall edge) based on an assumed rigid anchoring system. Wrapping of the wall with GFRP was simulated with 16 rows of 17 FRP truss elements horizontally oriented along the lower 1200 mm of the wall. These elements were connected to the concrete by means of bond-link elements, except at the extreme nodes at the wall edges, which were simulated as perfectly bonded due the wrapping of the FRP around the wall (Fig. 15). At the end of the initial analysis, the repair and retrofitting was simulated by engaging the elements corresponding to the vertical and horizontal FRP, including bond-link elements, and the elements defining the repaired concrete. Removing of concrete in the lower 250 mm of the web and boundary elements was simulated by disengaging the concrete elements originally present in this zone.

The original wall, MSW1, displayed a rounded hysteretic response (Fig. 16). The wall reached

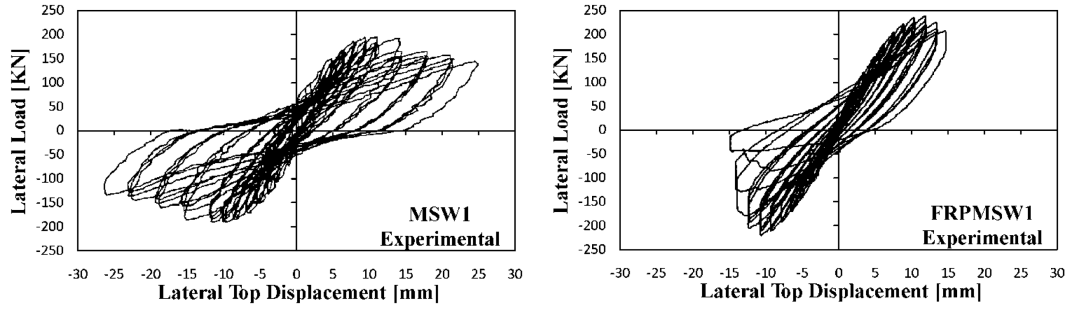

Fig. 16 Experimental load-deformation responses: (a) Wall MSW1 and (b) Wall FRPMSW1 (modified from Antoniades *et al.* 2005)

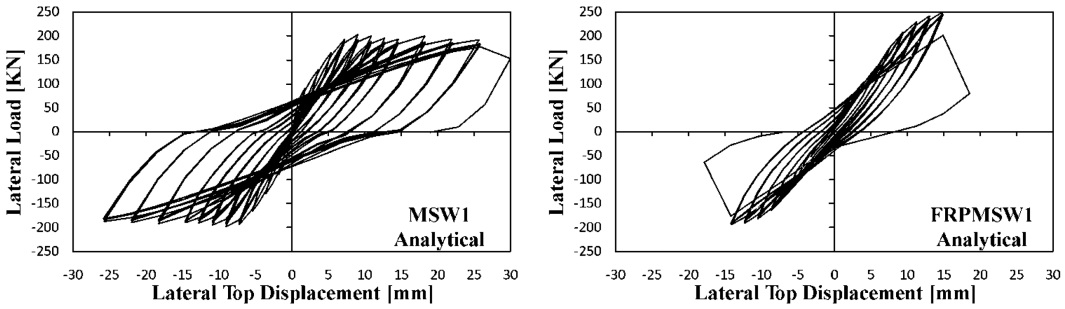

(a) (b)

Fig. 17 Numerical load-deformation responses: (a) Wall MSW1 and (b) Wall FRPMSW1

maximum lateral load capacity of 197 kN during the first repetition to 11 mm of displacement. During the post-peak, the wall experienced stiffness and strength degradation up to a maximum displacement of 26 mm, which corresponded to a displacement ductility of approximately 3.0. During the second repetition to 26 mm of displacement, the wall failed by shear sliding along the foundation beam. The hysteretic loops exhibited some pinching as a result of the shear stiffness degradation at the base of the wall; however, energy dissipation capacity was evident.

The repaired and retrofitted wall, FRPMSW1, responded with enhanced strength and similar initial stiffness to the original wall; however, the ductility and energy dissipation were reduced (Fig. 16). Maximum lateral load capacity of approximately 245 kN was attained at 12 mm of displacement, followed by strength degradation mainly due to concrete softening. The failure mechanism involved rupturing of the vertical FRP strip anchors at a lateral displacement of 15 mm. Subsequently, a complete loss of lateral load capacity resulted.

The predicted response of the original wall, MSW1, (Fig. 17) compared very well with the observed behaviour (Fig. 16). Characteristics of the response such as initial stiffness, lateral strength, unloading and reloading, and pinching were accurately captured. The analysis predicted a lateral strength of 203 kN at 9 mm of displacement. Beyond 15 mm, the response maintained the lateral load to approximately 25 mm of displacement, while strength degradation was more evident in the observed behaviour. This difference can be attributed to the assumed strain hardening of the vertical steel, which was not reported by Antoniades *et al.* (2005). However, the maximum lateral displacement of 26 mm prior failure was in good agreement. Failure in the form of shear sliding was adequately predicted. The predicted energy dissipation, although slightly higher than observed as a result of the strength overestimation in the post-peak response, was satisfactorily captured.

During preliminary analysis of the repaired/retrofitted wall, FRPMSW1, the strength was overestimated since failure as a consequence of the anchoring system of the vertical CFRP was not modelled. An improvement was obtained by disconnecting the vertical CFRP from the foundation beam during the third repetition of loading to 15 mm of displacement. The modified model predicted a response (Fig. 17) that was in good agreement with the observed behaviour. Failure was due to rupturing of the vertical reinforcing bars. A more detailed model of the anchor would provide a more accurate prediction of the failure mode. The ultimate strength of 251 kN was predicted at a displacement of 15 mm.

Table 1 Material properties of repaired/retrofitted walls

Wall	Zone	Concrete	Reinforcement					
			Horizontal		Vertical		Confinement	
		Old/New $f'c$ [MPa]	ρ_h [%]	fy [MPa]	ρ_v [%]	fy [MPa]	ρ_{cf} [%]	fy [MPa]
B11/B11R*	Web	53.8/42.6	0.63	501	0.29	501	—	—
	Boundary	53.8/—	1.35/0.33	501	3.67	429	1.35/0.13	501
LSW3/	Web	23.9/75	0.28	575	0.28	575	0.06	575
RLSW3	Boundary	23.9/75	1.03	575	1.26	585	0.86	575
SW24/	Web	37.9	0.56	400	0.63	545	—	—
SWR24**	Boundary	37.9	2.79/0.56	400	5.10	545	1.12/0.22	400
W11/W11RP***	Web	29	0.24	480	0.24	480	—	—
	Boundary	—	—	—	—	—	—	—
MSW1/	Web	26.1/75	0.57	585	0.57	585	0.06	575
FRPMSW1†	Boundary	26.1/75	0.66	575	1.68	585	0.55	575

*Two reinforcing bars No. 5 at 45 deg. in each direction added in the lower 90 cm, $fy = 501$ MPa.
**Nine staggered horizontal plates (78 × 3.6 mm), $fy = 275$ MPa; $f'c$ taken as 0.77 $fcub$.
***Two vertical steel plates (160 × 4.76 mm) near each end face of the wall.
†Three layers $tf = 0.45$ mm vertical CFRP, $fu = 1100$ MPa; one layers $tf = 0.60$ mm horizontal GFRP, $fu = 550$ MPa.

5. Conclusions

This paper presents results of shear walls modelled with the finite element method. Quick, simple, yet reliable modelling procedures were developed for shear walls repaired and retrofitted with different techniques ranging from conventional replacement of concrete to external bonding of FRP. Salient parameters of seismic response were assessed: maximum strength, maximum lateral displacement, failure mechanism, energy dissipation, stiffness, and hysteretic response. In general, strong correlation between the analytical and experimental results was demonstrated. Some discrepancies were obtained, specifically in those walls where information of the materials properties was either incomplete or not entirely clear. Generally, the response of shear walls with low aspect ratio was more difficult to capture, and this was magnified when a new material was added such as steel plates or FPR sheets. The finite element method was capable of modelling repair and retrofitting of shear walls effectively by using simple finite elements, demonstrating that accuracy of results is not necessarily sacrificed when using FEM procedures with low-powered elements. Bond-link elements performed well when modelling externally bonded FRP and steel plates; however, further investigations are required to model the effect of buckling of reinforcing bars and rocking mechanisms in the cyclic response of repaired and retrofitted shear walls. This study demonstrated that FEM procedures can provide accurate simulations of repaired and retrofitted shear walls given a good analysis program capable of retaining residual damage in the virgin shear walls, and with comprehensive models for material and structural behaviour.

Acknowledgements

This project was partially supported by the Canadian Seismic Research Network (CSRN). The authors also wish to express their gratitude to the Canadian Bureau for International Education (CBIE) for granting the Government of Canada Award to the first author.

References

Antoniades, K.K., Salonikios, T.N. and Kappos, A.J. (2003), "Cyclic tests on seismically damaged reinforced concrete walls strengthened using fiber-reinforced polymer reinforcement", *ACI Struct. J.*, **100**(4), 510-518.

Antoniades, K.K., Salonikios, T.N. and Kappos, A.J. (2005), "Tests on seismically damaged reinforced concrete walls repaired and strengthening using fiber-reinforced polymers", *J. Compos. Constr. - ASCE*, **9**(3), 236-246.

Aprile, A., Spacone, E. and Limkatanyu, S. (2001), "Role of bond in RC beams strengthened with steel and FRP plates", *J. Struct. Eng. - ASCE*, **127**(12), 1445-1452.

Arduini, M., Di Tommaso, A. and Nanni, A. (1997), "Brittle failure in FRP plate and sheet bonded beams", *ACI Struct. J.*, **94**(4), 363-370.

Collins, M.P. and Porasz, A. (1989), "Shear design for high strength concrete", *CEB Bulletin d'Information No. 193 - Design aspects of concrete*, 75-83.

Cortés-Puentes, W.L. (2009), "Nonlinear modelling and analysis of repaired and retrofitted shear walls", M.A.Sc. Thesis, Department of Civil Engineering, University of Ottawa, Ottawa, Canada, 226pp.

Eligehausen, R., Popov, E. and Bertero, V. (1983), "Local bond stress-slip relationship of deformed bars under generalized excitations", Report No. UCB/EERC-83/23, Earthquake Engineering Center, University of California, Berkeley.

Elnashai, A.S. and Salama, A.I. (1992), "Selective repair and retrofitting techniques for RC structures in seismic regions", Research Report ESEE/92-2, Engineering Seismology and Earthquake Engineering Section, Imperial College, London, England.

Elnashai, A.S. and Pinho, R. (1998), "Repair and retrofitting of RC walls using selective techniques", *J. Earthq. Eng.*, **2**(4), 525-568.

Fiorato, A.E., Oesterle, R.G. and Corley, W.G. (1983), "Behavior of earthquake resistant structural walls before and after repair", *J. Am. Concrete I.*, September-October 1983, 403-413.

He, X.G. and Kwan, A.K.H. (2001), "Modeling dowel action of reinforcement bars for finite element analysis of concrete structures", *Comput. Struct.*, **79**(6), 595-604.

Kupfer, H., Hilsdorf, H.K. and Rusch, H. (1969), "Behavior of concrete under biaxial stress", *J. Am. Concrete I.*, **66**(8), 656-666.

Li, Z.J., Balendra, T., Tan, K.H. and Kong, K.H. (2005), "Finite element modeling of cyclic behaviour of shear wall structure retrofitted using GFRP", *SP-230: 7th International Symposium on Fiber-Reinforced (FRP) Polymer Reinforcement for Concrete Structures*, *ACI*, 2005, 1305-1324.

Palermo, D. and Vecchio, F.J. (2003), "Compression field modeling of reinforced concrete subjected to reversed loading: formulation", *ACI Struct. J.*, **100**(5), 616-625.

Palermo, D. and Vecchio, F.J. (2007), "Simulation of cyclically loaded concrete structures based on the finite-element method", *J. Struct. Eng. - ASCE*, **133**(5), 728-738.

Park, R., Priestley, M.J.N. and Gill, W.D. (1982), "Ductility of square-confined concrete columns", *J. Struct. Eng. - ASCE*, **108** (4), 929-950.

Popovics, S. (1973), "A numerical approach to the complete stress-strain curve of concrete", *Cement Concrete Res.*, **3**(5), 583-599.

Richart, F.E., Brandtzaeg, A. and Brown, R.L. (1928), "A study of the failure of concrete under combined compressive stresses", Bulletin No.185, University of Illinois Engineering Experimental Station, Urbana, Illinois, 104pp.

Salonikios, T.N., Kappos, A.J., Tegos, I.A. and Penelis, G.G. (1999), "Cyclic load behavior of low-slenderness reinforced concrete walls: design basis and test results", *ACI Struct. J.*, **96**(4), 649-660.

Sato, Y. and Vecchio, F.J. (2003), "Tension stiffening and crack formation in reinforced concrete members with fiber-reinforced polymer sheets", *J. Struct. Eng. - ASCE*, **129**(6), 717-724.
Seckin, M. (1981), "Hysteretic behaviour of cast-in-place exterior beam-column-slab subassemblies", Ph.D. Thesis, Department of Civil Engineering, University of Toronto, Toronto, Canada, 266pp.
Smith, G.M. and Young, L.E. (1955), "Ultimate theory in flexure by exponential function", *J. Am. Concrete I.*, **52**(11), 349-359.
Taghdi, M., Bruneau, M. and Saatcioglu, M. (2000a), "Analysis and design of low-rise masonry and concrete walls retrofitted using steel strips", *J. Struct. Eng. - ASCE,* **126**(9), 1026-1032.
Taghdi, M., Bruneau, M. and Saatcioglu, M. (2000b), "Seismic retrofitting of low-rise masonry and concrete walls using steel strips", *J. Struct. Eng. - ASCE*, **126**(9), 1017-1025.
Vecchio, F.J. (1992), "Finite element modeling of concrete expansion and confinement", *J. Struct. Eng. - ASCE,* **118**(9), 46-56.
Vecchio, F.J. (1999), "Towards cyclic load modelling of reinforced concrete", *ACI Struct. J.*, **96**(2), 193-202.
Vecchio, F.J. (2000a), "Analysis of shear-critical reinforced concrete beams", *ACI Struct. J.*, **97**(1), 102-110.
Vecchio, F.J. (2000b), "Disturbed stress field model for reinforced concrete: formulation", *J. Struct. Eng. - ASCE*, **126**(9), 1070-1077.
Vecchio, F.J. and Bucci, F. (1999), "Analysis of repaired concrete structures", *J. Struct. Eng. - ASCE*, **125**(6), 644-652.
Vecchio, F.J. and Collins, M.P. (1986), "The modified compression-field theory for reinforced concrete elements subjected to shear", *J. Am. Concrete I.*, **83**(2), 219-231.
Vecchio, F.J. and Collins, M.P. (1993), "Compression response of cracked reinforced concrete", *J. Struct. Eng. - ASCE*, **119**(12), 3590-3610.
Vecchio, F.J. and Lai, D. (2004), "Crack shear-slip in reinforced concrete elements", *J. Adv. Concrete Technol.*, **2**(3), 289-300.
Vintzeleou, E.N. and Tassios, T.P. (1987), "Behavior of dowels under cyclic deformations", *ACI Struct. J.*, **84**(1), 18-30.
Wong, P.S. and Vecchio, F.J. (2002), "VecTor2 and formworks user's manual", *Technical Report,* Civil Engineering, University of Toronto, Toronto, Canada.

CC